

# X-ray Crystallographic Structure of the Norwalk Virus Capsid

B. V. Venkataram Prasad,<sup>1\*</sup> Michele E. Hardy,<sup>2†</sup>  
Terje Dokland,<sup>3‡</sup> Jordi Bella,<sup>3</sup> Michael G. Rossmann,<sup>3</sup>  
Mary K. Estes<sup>2</sup>

Norwalk virus, a noncultivable human calicivirus, is the major cause of epidemic gastroenteritis in humans. The first x-ray structure of a calicivirus capsid, which consists of 180 copies of a single protein, has been determined by phase extension from a low-resolution electron microscopy structure. The capsid protein has a protruding (P) domain connected by a flexible hinge to a shell (S) domain that has a classical eight-stranded  $\beta$ -sandwich motif. The structure of the P domain is unlike that of any other viral protein with a subdomain exhibiting a fold similar to that of the second domain in the eukaryotic translation elongation factor-Tu. This subdomain, located at the exterior of the capsid, has the largest sequence variation among Norwalk-like human caliciviruses and is likely to contain the determinants of strain specificity and cell binding.

Norwalk virus (NV) and Norwalk-like viruses (NLVs) are human caliciviruses (1) that account for over 96% of outbreaks of acute, nonbacterial gastroenteritis in the United States (2). These emerging, human pathogens are difficult to study because they remain refractory to cultivation in either tissue culture systems or animals. Native, infectious virions are difficult to characterize owing to the extremely low amount of virus excreted from humans. Virus is rarely seen unless stool samples are examined by immune electron microscopy (1). Successful cloning of the viral genome followed by production and purification of recombinant NV-like particles (3) have been instrumental in advancing the epidemiological, immunological, and biochemical properties of these viruses (4). However, further understanding of the viral replication strategies, pathogenesis, and immunity remains hindered by a lack of infectious molecular clones and cultivation systems. Recently, sequence analysis of NLVs has shown an unexpected diversity that may reflect a high number of serotypes, as seen for rhinoviruses, suggesting that antiviral drugs will be required to treat human calicivirus infections (2, 4). Knowledge of the atomic structure of these viruses now provides a

foundation for dissecting the antigenic properties of caliciviruses as well as providing insights into the molecular interactions that govern virus assembly and genome encapsidation. This structural information can guide mutational analyses to test new approaches for virus cultivation and could lead to the design of antiviral compounds.

Norwalk virus contains a single-stranded, positive-sense, RNA genome of about 7.7 kb (3) that is incorporated within a shell consisting of multiple copies of a single protein of ~56.6 kD (3, 5). Electron cryomicroscopy (cryo-EM) and computer image processing techniques have been used to study the three-dimensional structures of recombinant Norwalk virus (rNV) particles and two other animal caliciviruses at about 22 Å resolution (6). These studies have shown that caliciviruses exhibit a  $T = 3$  icosahedral symmetry with 180 molecules of the capsid protein organized into 90 dimers (Fig. 1A). The capsid has a contiguous protein shell between 100 and 145 Å radius, with prominent protrusions at all the local and strict twofold axes that extend to an outer radius of ~190 Å, leaving large depressions at the icosahedral five- and threefold axes. We report here the structure of the rNV capsid at near atomic resolution as determined by x-ray crystallography. Crystals of the rNV particles diffracted to at least 3.2 Å resolution by synchrotron radiation. The x-ray phasing was accomplished to 3.4 Å resolution (Fig. 1B) by electron density averaging starting with the cryo-EM structure as an initial phasing model (7).

The structure of the capsid protein, which exhibits both classical and novel features, can be described as having two principal domains, S and P, linked by a flexible hinge

(Fig. 1, C and D). The S domain is involved in the formation of the icosahedral shell, and the P domain forms the prominent protrusion emanating from the shell. The NH<sub>2</sub>-terminal 225 residues constitute the S domain. Residues 50 to 225 fold into a classical eight-stranded antiparallel  $\beta$  sandwich, a common fold seen in many viral capsid proteins. The eight  $\beta$  strands, conventionally denoted as B to I, are organized into two sheets, BIDG and CHEF, in a manner similar to that seen in other proteins with this fold. The two  $\alpha$  helices ( $\alpha$ A and  $\alpha$ B), frequently associated with this fold, are positioned between the C and D, and E and F strands, respectively. The loop that connects the E and F strands has a Pro-Pro-Gly sequence that is conserved among different NLV strains. This sequence is also conserved in the structural proteins, VP1, VP2, and VP3 of several picornaviruses, as a part of the E-F loop (8). This motif, located near the quasi threefold axis of each icosahedral asymmetric unit, may have a structural role in maintaining appropriate intersubunit contacts.

The fold of the P domain, formed by residues 225 to the COOH-terminus, is unlike that of any other viral protein. This domain is made of two subdomains: P1, consisting of residues 226 to 278 and 406 to 520; and P2, consisting of residues 279 to 405 (Fig. 1C). The P2 subdomain is a large insertion between the residues 278 and 406. Residues 285 to 380 in the P2 subdomain fold into a compact barrel-like structure consisting of six  $\beta$  strands. The fold of the polypeptide in this domain, as indicated by the program DALI (9), is similar to that seen in the RNA binding domain 2 (residues 215 to 307) of the elongation factor-Tu (EF-Tu), a GTP binding protein involved in transporting aminoacyl-tRNAs to ribosomes (10). The root mean square deviation [calculated with the procedure described in (11)] between the matching 62 C $\alpha$  atoms (out of 92 residues) was ~2.9 Å. This similarity suggests a possible role for the P2 subdomain in viral or cellular RNA translation and regulation of protein synthesis.

Within the P1 subdomain, residues 226 to 278 contain three short stretches of  $\beta$  strands, whereas the COOH-terminal 114 residues contain six  $\beta$  strands and a well-defined  $\alpha$  helix. Although no statistically significant scores were obtained when the whole P1 or the COOH-terminal portion alone was compared with other proteins in the Protein Database [with the DALI program (9)], the folding pattern is not entirely unique. The residues from 450 to 490 containing four  $\beta$  strands form a twisted antiparallel  $\beta$  sheet having a Greek-key motif (12) in which the fourth strand folds back to interact with the first strand.

To form a  $T = 3$  icosahedral structure, the capsid protein has to adapt to three quasi-equivalent positions. The subunits at these positions are conventionally referred to as A,

<sup>1</sup>Verna and Marrs Mclean Department of Biochemistry, <sup>2</sup>Division of Molecular Virology, Baylor College of Medicine, Houston, TX 77030, USA. <sup>3</sup>Department of Life Sciences, Purdue University, West Lafayette, IN 47907, USA.

\*To whom correspondence should be addressed. E-mail: vprasad@bcm.tmc.edu

†Present address: Veterinary Molecular Biology, Montana State University, Bozeman, MT 59717, USA.

‡Present address: Institute of Molecular Agrobiolgy, National University of Singapore, Singapore 117604.

## REPORTS

B, and C (13). In the modular structure of the capsid protein, the S domain is involved in the icosahedral contacts (Fig. 2A), whereas the P domain is exclusively involved in the dimeric contacts (Fig. 2B). The P domains of the A and B subunits interact across the quasi twofold axes to form the dimeric protrusions as seen in the cryo-EM reconstruction (Fig. 1A). Similarly, the P domains of the C subunits interact across the icosahedral twofold axes. The A/B and C/C dimers are stabilized mainly by interactions between the side chains of the participating monomers with a total contact area of about 2000 Å<sup>2</sup>.

The packing of the S domains of an A/B dimer has a "bent" conformation, whereas in the C/C dimer the packing has a "flat" conformation (Fig. 2B). Switching between the "bent" and the "flat" conformations, as seen in other  $T = 3$  viruses (13, 14), facilitates the

appropriate curvature for the formation of a closed shell. Although the packing of the S domains in the rNV capsid is very similar to that in other  $T = 3$  and  $P = 3$  (pseudo  $T = 3$ ) viruses, the mechanism of mediating the local curvature in the icosahedral shell appears to be different. In the other  $T = 3$  viruses, the dimeric S domains pivot about an axis parallel to the  $\alpha A$  helix, perpendicular to the dimeric axis, dividing the A/B and C/C contacts above and below the pivot axis, respectively. In plant viruses, such as tombus and sobomo viruses (15, 16), the  $\beta A$  arm (NH<sub>2</sub>-terminal extension of the  $\beta B$  strand in the  $\beta$  sandwich) of the C subunit is wedged between the opposing S domains of the C/C dimer, to keep the C-C contacts flat. In the insect nodaviruses, a portion of the genomic RNA and a small ordered NH<sub>2</sub>-terminal portion of the COOH subunit keep the C/C

dimers flat (17). In the Norwalk capsid, the S domains undergo small, localized conformational changes to maintain essentially the same interactions between the opposing S domains in both A/B and C/C dimers. The residues 49 to 54 (equivalent of  $\beta A$ ) in the NH<sub>2</sub>-terminal arm, and the  $\alpha A$  helix participate in these interactions in both the dimers. The  $\beta A$  strand is essentially a continuation of the  $\beta B$  strand separated by a kink, instead of a distinct strand of opposite polarity as seen in the C subunits of  $T = 3$  plant viruses (Fig. 2C). Pivoting about an axis parallel to the  $\alpha A$  helix, together with an azimuthal rotation of the S domains with respect to the P domains facilitated by the hinge between the S and P domains, imparts the differential curvatures to the A/B and C/C dimers.

The structures of A and B subunits remain essentially the same, maintaining a similar

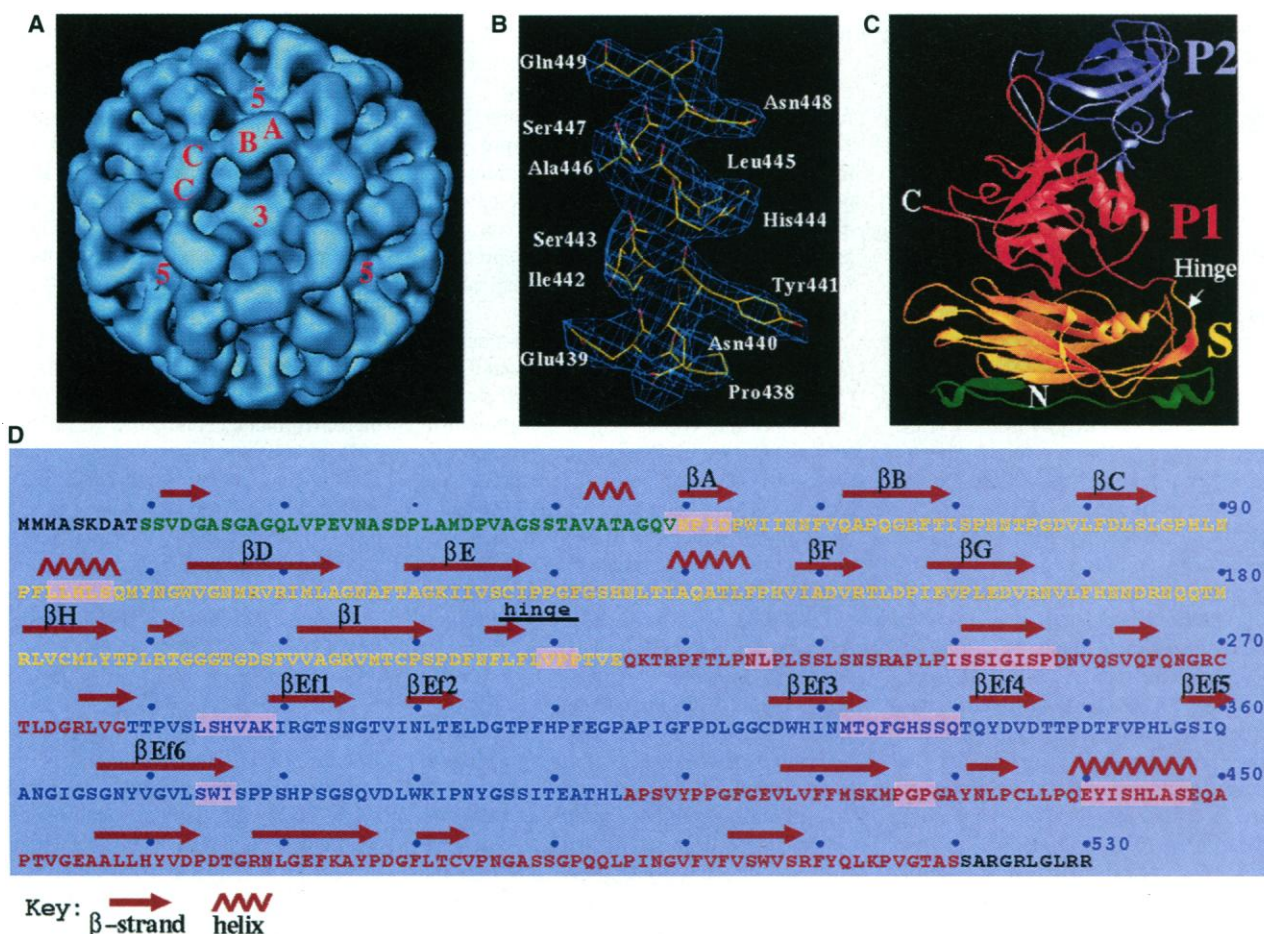


**Fig. 1.** (A) Three-dimensional structure, as viewed along the icosahedral threefold axis, of the rNV capsid at 22 Å resolution as determined by cryo-EM techniques. This structure was used as a model for initial phasing of the x-ray data. The locations of the A, B, and C subunits (see also Fig. 2A) are indicated. (B) A representative sample of the electron density map at 3.4 Å resolution with the modeled structure (residues 438 to 449). (C) A ribbon representation of the structure of the rNV capsid protein (B subunit). The NH<sub>2</sub>-terminal arm (residues 10 to 49), which faces the interior of the capsid, is shown in green; the S domain (residues 50 to 225), in yellow; the P1 subdomain (residues 226 to 278, and residues 406 to 520), in red; and the P2 subdomain (residues 279 to 405),

in blue. In this orientation of the subunit structure, the right-hand side of the P domain is involved in dimeric contacts and the left-hand side faces the hollows in the capsid structure. (D) Sequence and structure analysis of the rNV capsid protein. The color coding of the various domains is as in (C). Regions involved in the dimer contacts are shaded pink, disordered regions are shown in black. The  $\beta$  strands in the eight-stranded  $\beta$  sandwich fold are indicated by letters B to I, and those in the P2 subdomain are suffixed by Ef. Every 10th residue is indicated by a dot on top. Abbreviations for the amino acid residues are as follows: A, Ala; C, Cys; D, Asp; E, Glu; F, Phe; G, Gly; H, His; I, Ile; K, Lys; L, Leu; M, Met; N, Asn; P, Pro; Q, Gln; R, Arg; S, Ser; T, Thr; V, Val; W, Trp; and Y, Tyr.

## REPORTS

relative orientation between the S and P domains. The difference between the two subunits is mainly in the NH<sub>2</sub>-terminal residues. In the B subunit, the NH<sub>2</sub>-terminal nine residues are disordered, whereas in the A subunit (and also in C), the NH<sub>2</sub>-terminal 29 residues are disordered. The ordered NH<sub>2</sub>-terminal residues of the B subunit interact with the  $\beta$ F strand in the S domain of the neighboring C subunit around the icosahedral threefold axis (Fig. 2C). The observed hydrogen bond interactions between the P1 (residues 505 and 506) and the S (residues 64 and 65) domains in the A and B subunits may be necessary for maintaining the "bent" conformation of the A/B dimer. These interactions are absent in the C/C dimer because of the change in the relative orientation between the S and P domains. The "flat" conformation of the C/C dimer might be stabilized by the interactions with the ordered NH<sub>2</sub>-terminal residues of the neighboring B subunits.

Sequence comparisons between the capsid proteins of genetically distinct human calicivirus strains (4) indicate that the S domain represents the most conserved region of the sequence. Whereas the P1 subdomain is moderately well conserved, the highly variable part of the sequence be-

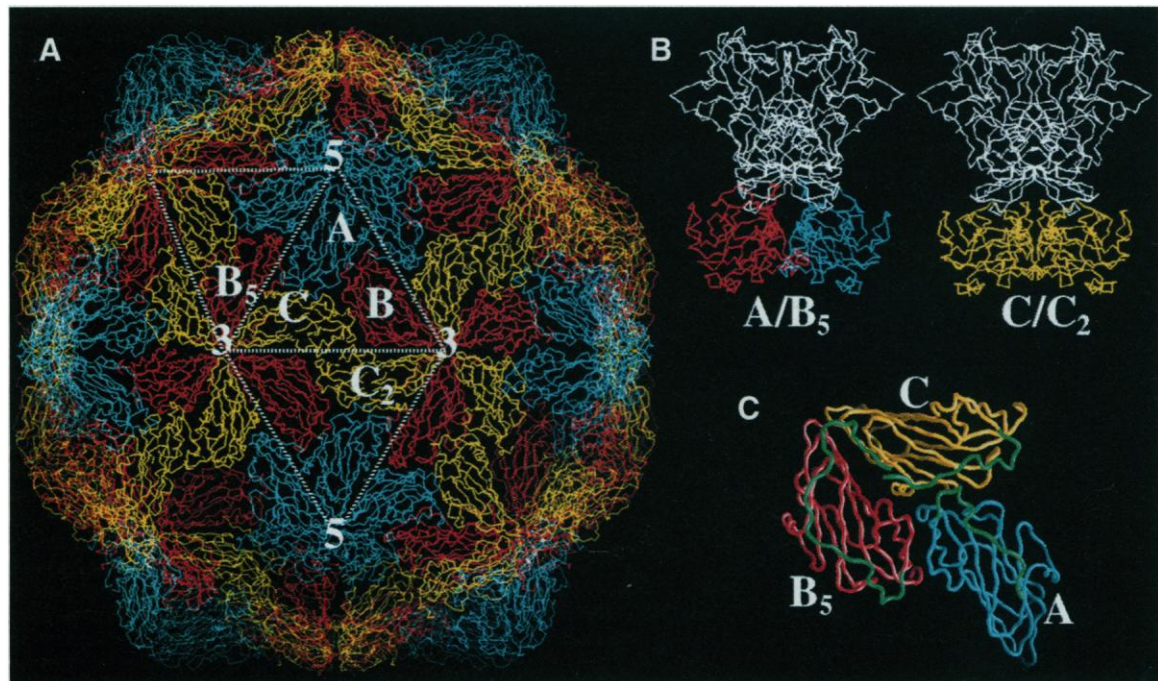
tween residues 280 and 400 is in the P2 subdomain, which is the most exposed region of the structure. Therefore, this region may contain the determinants of strain specificity. Presently there are no data on how these viruses interact with the host cells. However, it has been shown that a monoclonal antibody that recognizes a region between the residues 300 and 384 in the P2 subdomain inhibits binding of rNV capsids to cells (18), suggesting that the P2 subdomain is also involved in cell binding activity.

Mutational analysis indicates that the deletion of the entire P domain inhibits particle assembly and the dimer formation (19). The rNV structure shows that most of the interactions between monomers that constitute a dimer reside in the P domain. These observations suggest that the dimers are likely to be formed before capsid assembly. The large contact area,  $\sim 1800 \text{ \AA}^2$ , between the symmetry-related S domains of the A/B dimers around the fivefold axis suggests that pentamers of dimers are likely formed as intermediates in the assembly pathway. The dimers may coexist in the two conformational states seen in the capsid structure. The "bent" A/B dimers associate to form the pentamers,

which are then joined together by the inclusion of "flat" C/C dimers to complete the assembly (Fig. 3). The NH<sub>2</sub>-terminal residues of the B subunits in the pentamer of A/B dimers may provide a switch for selectively incorporating the C/C dimers in this process. A similar assembly pathway from pentamers of A/B dimers has been suggested for southern bean mosaic virus (20). An alternative pathway with trimers of C/C dimers, as proposed for tombus viruses (21), is less likely because there are no significant contacts between the threefold related C/C dimers in the NV capsid.

Particle assembly is not linked to protein-RNA interactions because the recombinant capsid protein readily assembles without the genomic RNA. Because of the absence of appropriate sized holes in the capsid structure, it is unlikely that the RNA is encapsidated after the capsid assembly. Instead, the genome packaging could be concomitant with capsid assembly. The NH<sub>2</sub>-terminus of the NV capsid protein, located in the interior of the particles, as in many other  $T = 3$  and  $P = 3$  virus structures, lacks a predominance of basic residues and therefore may not directly play a role in the encapsidation of the viral genome. Possibly, the highly basic pro-

**Fig. 2.** (A) Interactions between the S domains in the icosahedral shell of the rNV capsid. The S domains of the three quasi-equivalent subunits, A, B, and C, which constitute the asymmetric unit of the  $T = 3$  lattice, are colored in blue, red, and yellow, respectively. The asymmetric unit is indicated by a triangle along with the locations of the five- and threefold axes. Application of the icosahedral symmetry elements generates all 60 asymmetric units of the lattice. Five- and twofold related asymmetric units, namely B (subscripted by 5) and C (subscripted by 2) subunits, respectively, are also shown. The A



and B subunits of the fivefold related asymmetric units interact across the quasi twofold axis (mid-point of the line joining icosahedral three- and fivefold axes) to form the A/B dimer. Similarly, the two C subunits related by the icosahedral twofold axis form the C/C dimer. For clarity the P domains are not shown. (B) The A/B (left) dimer as viewed along the line joining the icosahedral three- and fivefold axes; and the C/C dimer (right) as viewed along the line joining the adjacent icosahedral threefold axes. In both cases, the dimeric twofold axis is vertical. The bent and the flat contacts of the opposing S domains of the A/B and the C/C dimers are clearly seen in this view. To superimpose the P domains of A/B with those of C/C, the C/C dimer has to be rotated by

8° about the dimeric twofold axis. (C) The NH<sub>2</sub>-terminal residues (shown in green) of the three subunits (in tapeworm representation) as viewed from inside the capsid structure. Residues 10 to 14 of the NH<sub>2</sub>-terminal arm of the B subunit interact with the  $\beta$ F strand of the CH $\beta$ F sheet in the neighboring C subunit. The position of this inserted arm of the B subunit forces the NH<sub>2</sub>-terminal residues of the C subunit to be disordered and helps impose the threefold symmetry on the interactions around the quasi sixfold position. The dimer contacts involving  $\alpha$ A helix and  $\beta$ A strand between the S domains of A/B are shown in this view. The color coding of the S domains in (B) and (C) is the same as in (A), and the P domains are shown in white.

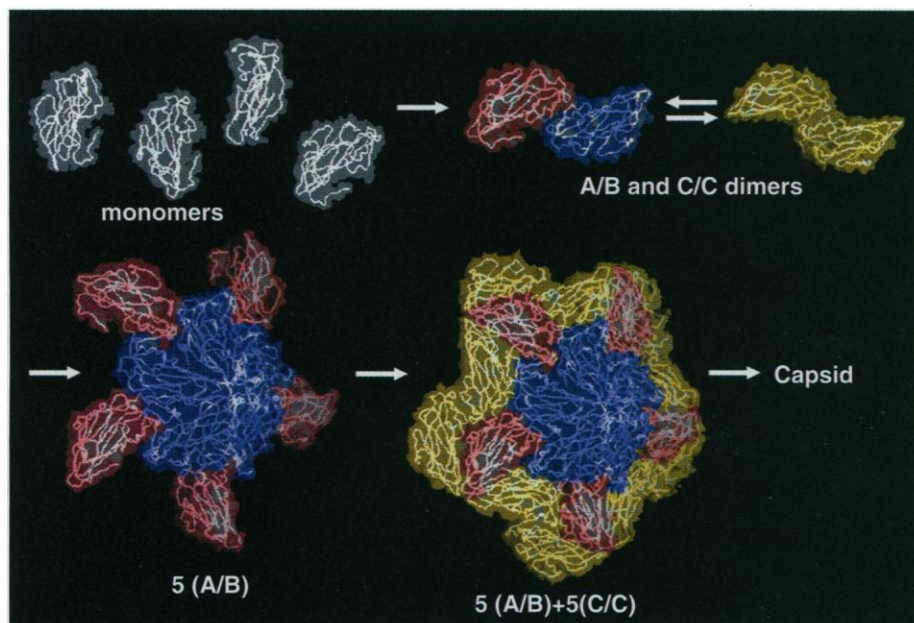


**Fig. 3.** A proposed assembly pathway. For simplicity, only the S domains are shown. The color scheme is the same as in Fig. 2A.

tein encoded by the open reading frame 3 of the viral genome, which has recently been shown to be a minor structural component in an animal calicivirus (22) and in the Norwalk virus (23), is involved in RNA encapsidation.

In summary, the first atomic structure of a calicivirus has been determined by combining cryo-EM and x-ray crystallographic techniques. Compared with other  $T = 3$  and  $P = 3$  viruses, the architecture of NV closely resembles that of the plant tombus viruses (15), which also have a well-defined shell domain and a protruding domain. The S domains of the tombus viruses, like those of NV, have the classical eight-stranded  $\beta$  sandwich. However, there is little resemblance in the topology of their P domains. Whereas the P domains of tombus viruses have a 10-stranded antiparallel  $\beta$ -sandwich structure, part of the P domain of the NV capsid protein contains a fold similar to the domain 2 of EF-Tu protein. Further studies are required to establish if there is a functional significance to this EF-Tu-like fold in the NV capsid protein. Although the structural features and the domain organization that is seen in the NV capsid are likely to be conserved across all human calicivirus strains, the P2 subdomain, which is an elaborate insertion in the P1 subdomain, may serve as a replaceable module to facilitate strain diversity.

#### References and Notes

1. A. Z. Kapikian, M. K. Estes, R. M. Channock, in *Virology*, B.N. Fields et al., Eds. (Lippincott-Raven, New York, 1996), vol. 1, pp. 783–810.
2. R. L. Fankhauser et al., *J. Infect. Dis.*, **178**, 1571 (1998).
3. X. Jiang, D. Y. Graham, K. N. Wang, M. K. Estes, *Science* **250**, 1580 (1990); S. M. Matsui et al., *J. Clin. Invest.* **87**, 1456 (1991); P. R. Lambden, E. O. Caul, C. R. Ashley, I. N. Clarke, *Science* **259**, 516 (1993); X.

- Jiang, M. Wang, K. Wang, M. K. Estes, *Virology* **195**, 51 (1993); X. Jiang, M. Wang, D. Y. Graham, M. K. Estes, *J. Virol.* **66**, 6527 (1992).
4. M. K. Estes and M. E. Hardy, in *Infections of the Gastrointestinal Tract*, M. J. Blaser et al., Eds. (Raven, New York, 1995), pp. 1009–1034.
5. H. B. Greenberg et al., *J. Virol.* **37**, 994 (1981).
6. B. V. V. Prasad, R. Rothnagel, X. Jiang, M. K. Estes, *ibid.* **68**, 5117 (1994); B. V. V. Prasad, D. O. Matson, A. W. Smith, *J. Mol. Biol.* **240**, 256 (1994); E. Thouvenin et al., *ibid.* **270**, 238 (1997).
7. Preparation of the rNV particles and image reconstruction at 22 Å resolution were as described in (6). The particles, purified on 10 to 50% (w/v) sucrose gradients in MilliQ water, were centrifuged for 2 hours at 130,000g, and the pellet was suspended in MilliQ water at a concentration of ~10 mg/ml. Crystals of the rNV particles suitable for x-ray structure determination were grown by the hanging drop method with 0.5 M ammonium phosphate (pH 4.8) as the precipitant. X-ray data were collected at CHESS on the F1 station (wavelength  $\lambda = 0.908$  Å). Oscillation data from 50 crystals were processed, scaled, and postrefined with the procedures described [M. G. Rossmann, *Acta Crystallogr.* **12**, 225 (1979); \_\_\_\_\_, A. G. W. Leslie, S. S. Abdel-Meguid, T. Tsukihara, *J. Appl. Crystallogr.* **12**, 570 (1979)]. The unit cell dimensions of the crystal were  $a = 605.7$  Å,  $b = 605.7$  Å,  $c = 466.7$  Å in the space group  $P4_22_12$ . The data (685316 unique reflections from 35 to 3.2 Å resolution, with 50% completeness; and 54% between 5 and 3.4 Å) merged with an  $R$  factor of 12.6%. The particle orientation in the unit cell was determined with a self-rotation function [M. G. Rossmann and D. M. Blow, *Acta Crystallogr.* **15**, 24 (1962); L. A. Tong and M. G. Rossmann, *Acta Crystallogr.* **A**, **46**, 783 (1990)] and particle position was found by translation function calculations with the cryo-EM structure as the model. The asymmetric unit of the crystal contains half a particle, with one of the icosahedral twofold axes of the particle coincident with a crystallographic twofold axis; as a result, the noncrystallographic redundancy is 30-fold. The cryo-EM structure was used for obtaining the initial phases. Carbon atoms with a temperature factor of 500 Å<sup>2</sup> were placed at all the grid points (spaced 5 Å apart) whose density values were above a selected threshold in the cryo-EM map. The phases were refined by real space

electron density averaging with icosahedral symmetry elements and solvent flattening. Phase extension and refinement was carried out gradually in steps of one reciprocal lattice point by iterative cycles of molecular averaging, solvent flattening, and back transformation as described [M. G. Rossmann et al., *J. Appl. Crystallogr.* **25**, 166 (1992)]. A radial mask with an internal radius of 95 Å and an external radius of 200 Å was used during the phase extension. The entire phase extension to 3.4 Å resolution took 138 steps, and each step included at least five cycles of noncrystallographic 30-fold averaging. At 3.4 Å resolution, the overall correlation-coefficient was 0.85 with an  $R$  factor of 20% (0.54 and 29%, in the highest resolution shell). The electron density map was of good quality and allowed interpretation in terms of the secondary and tertiary structures of all the quasi-equivalent subunits. Atomic models, including the side chains of the three quasi-equivalent subunits, were built into the electron density map with the program O [T. A. Jones, J.-Y. Zou, S. W. Cow, M. Kjeldgaard, *Acta Crystallogr.* **A47**, 110 (1991)]. After positional and  $B$ -factor refinement with *X-PLOR* [A. T. Brunger, Yale University Press, CT (1992)], the  $R$  factor decreased from an initial value of 33 to 26% for all the data to 3.4 Å resolution. After the refinement, the stereochemistry of the structure was checked with PROCHECK [R. A. Laskowski et al., *J. Appl. Crystallogr.* **26**, 283 (1993)]; 85% of the nonglycine residues were within the most favored regions, and none of the residues were in the disallowed regions. Other stereochemical characteristics of the three subunits are comparable with those of other structures determined to ~3.0 Å resolution. GRASP software [A. Nicholls, R. Bharadwaj, B. Honig, *Biophys. J.* **64**, A166 (1993)] was used for calculating buried surface area and for making Figs. 2C and 3.

8. A. C. Palmenberg, in *Molecular Aspects of Picornavirus Infection and Detection*, B. Semler and E. Ehrenfeld, Eds. (American Society of Microbiology, Washington, DC, 1989), pp. 211–241; M. Luo et al., *Science* **235**, 182.
9. M. Kjeldgaard, P. Nissen, S. Thirup, J. Nyborg, *Structure* **1**, 35 (1993); V. Hornung, H.-P. Hofmann, M. Sprinzl, *Biochemistry* **37**, 7260 (1998).
10. L. Holm and C. Sander, *J. Mol. Biol.* **233**, 123 (1993). The  $Z$  score between the P2 subdomain and the EF-Tu domain was 3.5.
11. S. T. Rao and M. G. Rossmann, *J. Mol. Biol.* **76**, 241 (1973).
12. J. S. Richardson, *Methods Enzymol.* **115**, 349 (1985).
13. M. G. Rossmann and J. E. Johnson, *Annu. Rev. Biochem.* **58**, 533 (1989).
14. S. Harrison, J. J. Skehel, D. Wiley, in *Virology*, B. N. Fields et al., Eds. (Raven, New York, 1996), vol. 1, pp. 59–99.
15. S. C. Harrison et al., *Nature* **276**, 368 (1978); J. M. Hogle, A. Maeda, S. C. Harrison, *J. Mol. Biol.* **191**, 625 (1986).
16. C. Abad-Zapatero et al., *Nature* **286**, 33 (1980).
17. A. J. Fisher and J. E. Johnson, *Nature* **361**, 176 (1993); J. P. Wery, V. S. Reddy, M. V. Hosur, J. E. Johnson, *J. Mol. Biol.* **235**, 565 (1994).
18. L. J. White et al., *J. Virol.* **70**, 6589 (1996).
19. L. White, thesis, Baylor College of Medicine, Houston, TX (1997).
20. M. G. Rossmann, C. Abad-Zapatero, M. A. Hermodson, J. W. Erickson, *J. Mol. Biol.* **166**, 37 (1983).
21. P. K. Sorger, P. G. Stockley, S. C. Harrison, *ibid.* **191**, 639 (1986).
22. C. Wirblich, H. J. Thiel, G. Meyers, *J. Virol.* **70**, 7974 (1996).
23. P. Glass and M. K. Estes, unpublished results.
24. We thank the staff of the Cornell High Energy Synchrotron Source (CHESS) for assistance with data collection; M. Vyas, T. Schmidt, and R. McKenna for help with data collection and data processing; and M. F. Schmid for helpful comments on the manuscript. Supported by grants from NIH (to M.K.E., B.V.V.P., and M.G.R.) and a grant from the R. Welch Foundation (to B.V.V.P.).

6 May 1999; accepted 31 August 1999

## LINKED CITATIONS

- Page 1 of 1 -



*You have printed the following article:*

### **X-ray Crystallographic Structure of the Norwalk Virus Capsid**

B. V. Venkataram Prasad; Michele E. Hardy; Terje Dokland; Jordi Bella; Michael G. Rossmann; Mary K. Estes

*Science*, New Series, Vol. 286, No. 5438. (Oct. 8, 1999), pp. 287-290.

Stable URL:

<http://links.jstor.org/sici?sici=0036-8075%2819991008%293%3A286%3A5438%3C287%3AXCSOTN%3E2.0.CO%3B2-9>

---

*This article references the following linked citations:*

## References and Notes

### <sup>3</sup> **Norwalk Virus Genome Cloning and Characterization**

Xi Jiang; David Y. Graham; Kening Wang; Mary K. Estes

*Science*, New Series, Vol. 250, No. 4987. (Dec. 14, 1990), pp. 1580-1583.

Stable URL:

<http://links.jstor.org/sici?sici=0036-8075%2819901214%293%3A250%3A4987%3C1580%3ANVGCAC%3E2.0.CO%3B2-H>

### <sup>3</sup> **Sequence and Genome Organization of a Human Small Round-Structured (Norwalk-Like) Virus**

Paul R. Lambden; E. Owen Caul; Charles R. Ashley; Ian N. Clarke

*Science*, New Series, Vol. 259, No. 5094. (Jan. 22, 1993), pp. 516-519.

Stable URL:

<http://links.jstor.org/sici?sici=0036-8075%2819930122%293%3A259%3A5094%3C516%3ASAGOOA%3E2.0.CO%3B2-0>

### <sup>8</sup> **The Atomic Structure of Mengo Virus at 3.0 Å Resolution**

Ming Luo; Gerrit Vriend; Greg Kamer; Iwona Minor; Edward Arnold; Michael G. Rossmann; Ulrike Boege; Douglas G. Scraba; Greg M. Duke; Ann C. Palmenberg

*Science*, New Series, Vol. 235, No. 4785. (Jan. 9, 1987), pp. 182-191.

Stable URL:

<http://links.jstor.org/sici?sici=0036-8075%2819870109%293%3A235%3A4785%3C182%3ATASOMV%3E2.0.CO%3B2-6>

**NOTE:** *The reference numbering from the original has been maintained in this citation list.*